http://dx.doi.org/10.1117/12.2081348

Which Pivot Calibration?

Ziv Yaniv

Office of High Performance Computing and Communications, National Library of Medicine, National Institutes of Health, Bethesda, MD, 20894, USA

ABSTRACT

Estimating the location of a tracked tool's tip relative to its Dynamic Reference Frame (DRF) and localizing a specific point in a tracking system's coordinate frame are fundamental tasks in image-guided procedures. The most common approach to estimating these values is by pivoting a tool around a fixed point. The transformations from the tracking system's frame to the tool's DRF are the input. The output is the translation from the DRF to the tool's tip and the translation from the tracker's frame to the pivoting point. While the input and output are unique, there are multiple mathematical formulations for performing this estimation task. The question is, are these formulations equivalent in terms of precision and accuracy? In this work we empirically evaluate three common formulations, a geometry based sphere fitting formulation and two algebraic formulations. In addition we evaluate robust variants of these formulations using the RANSAC framework. Our evaluation shows that the algebraic formulations yield estimates that are more precise and accurate than the sphere fitting formulation. Using the Vicra optical tracking system from Northern Digital Inc., we observed that the algebraic approaches have a mean(std) precision of 0.25(0.11)mm localizing the pivoting point relative to the tracked DRF, and yield a fiducial registration error with a mean(std) 0.15(0.08)mm when registering a precisely constructed divot phantom to the localized points in the tracking system's frame. The sphere fitting formulation yielded less precise and accurate results with a mean(std) of 0.35(0.21)mm for precision and 0.25(0.14)mm for accuracy. The robust versions of these formulations yield similar results even when the data is contaminated with 30% outliers.

Keywords: calibration, localization and tracking technologies, validation and evaluation

1. INTRODUCTION

What does the calibration of a pointer tool have in common with estimating the spatial location of a patient's femur head center? Both of these tasks can be performed using pivot calibration.

We formally define pivot calibration as the following estimation task. Given a set of rigid transformations $[R_i, \mathbf{t}_i]_{i=1..m}$ obtained by pivoting a tracked object around a fixed world point, estimate the translation, ${}^{DRF}\mathbf{t}$, from the Dynamic Reference Frame (DRF) origin to the pivoting point and the translation, ${}^{W}\mathbf{t}$, from the world/tracker origin to the pivoting point. Figure 1 shows the coordinate systems and transformations involved in this process.

This approach to point localization is primarily used for calibrating tools, but has also been used for localizing anatomy. As tool calibration is a ubiquitous task in image-guided procedures, pivot calibration has been previously described in a large number of publications. The following are a representative selection.

Estimating the tip location of a pointer tool with respect to a rigidly attached DRF is the most common usage of pivot calibration. This technique was described in.[1–3] Once calibrated, the pointer tool is used to digitize various points, primarily for registration between preoperative images and the intraoperative setting. Calibration of tools that are geometrically similar to a pointer such as RFA probes, biopsy needles, and kyphoplasty introducer devices were described in.[4–6] In this case the need for calibration stems from the desire to overlay the tool tip in its correct location on preoperative images after they have been registered to the intraoperative setting. An example of calibrating a "virtual" pointer tool was described in.[7] In this case, the interaction point of a PHANToM haptic device is localized with respect to a DRF attached to the device's stylus. Rotating the stylus around a point is performed by rendering a fixation force such that the haptic interaction point remains fixed

E-mail: zivyaniv@nih.gov

Medical Imaging 2015: Image-Guided Procedures, Robotic Interventions, and Modeling,
edited by Ziv R. Yaniv, Robert J. Webster III, Proc. of SPIE Vol. 9415, 941527
© 2015 SPIE · CCC code: 1605-7422/15/$18 · doi: 10.1117/12.2081348

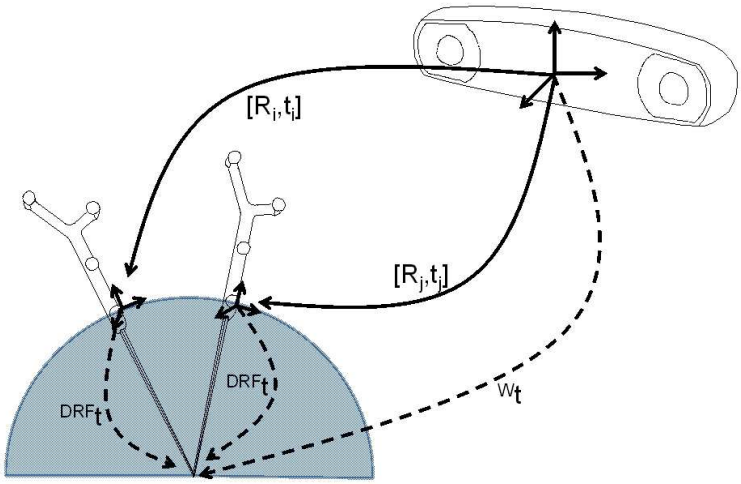

Figure 1. Pivot based calibration of a pointer tool, coordinate systems and transformations. Solid lines denote known transformations, dashed lines denote unknown translations. The origin of the coordinate system defined by the tool's Dynamic Reference Frame lies on a sphere in the tracker's coordinate system whose center is ${}^{W}\mathbf{t}$ and radius is $\|{}^{DRF}\mathbf{t}\|$.

in space. Once calibrated, the device provides realistic tactile feedback that is spatially correct with respect to virtual objects displayed in an augmented reality environment.

In the context of robotic total knee replacement surgery, pivot calibration was used to determine the center of the femur head.[8,9] In this procedure, the robot is physically attached to the knee and serves as the tracking system while the leg is rotated. The center of the femur head is localized in the robot's reference frame via pivot calibration, enabling the use of this anatomical point as a registration fiducial. This approach was later utilized in the context of image-less computer assisted total knee replacement surgery.[10,11] In this case, the leg's mechanical axis is determined by attaching optically tracked DRFs to the pelvis, femur, tibia and foot. The location of the center of the femur head, the knee and the ankle are all obtained via separate pivot calibrations.

In the general domain of robotics the use of pivot calibration as a method for determining a tool tip relative to a robot's coordinate frame via pivoting was described in.[12] The specific context for this calibration is not provided. In the context of medical robotics, examples include using pivot calibration to localize the tip of a drill bit held by the robot,[13] and localizing the tip of a needle holder held by the robot.[14] In both cases localization is with respect to a reference frame attached to the robot.

Two, less common, uses of pivot calibration are described in[15] and.[16] In the former case, pivot calibration is used to evaluate the tracking variability of an electromagnetic localization system in the context of 3D ultrasound. The standard deviation of the coordinates of the pivoting point location in the tracker's coordinate system are used as a measure of the tracker's precision. In the later case, pivot calibration is used as part of an ultrasound calibration approach.

While all of the publications use the same pivoting approach to calibration, they do differ in the mathematical formulation. We identified three common formulations: a geometry based Sphere Fitting (SF) formulation;[10,12] an Algebraic, One Step, (AOS) formulation;[5,15] and an Algebraic, Two Step, (ATS) formulation.[2,3] In this work we empirically evaluate these formulations in terms of precision and accuracy.

2. METHODS

A key difference between the formulations is the order in which they estimate the two translations. The SF formulation starts by estimating ${}^{W}\mathbf{t}$ via sphere fitting followed by estimating ${}^{DRF}\mathbf{t}$. The AOS formulation simultaneously estimates ${}^{W}\mathbf{t}$ and ${}^{DRF}\mathbf{t}$ as a solution to a single equation system. Finally, the ATS formulation starts by estimating ${}^{DRF}\mathbf{t}$ as a solution to an equation system followed by estimating ${}^{W}\mathbf{t}$.

While all three formulations estimate the same quantities using different approaches, they are all based on least-squares formulations and therefore sensitive to outliers. This common deficiency is readily addressed as will be described below. We next describe all formulations using a common notation.

2.1 Mathematical formulations

2.1.1 Sphere Fitting (SF)

This formulation is based on the observation that the locations of the DRF, the translational component of the input transformations $[R_i, \mathbf{t}_i]_{i=1..m}$, are all on the surface of a sphere whose center is ${}^{W}\mathbf{t}$.

To estimate the sphere center we use a least squares formulation,[17] initially using an analytic estimate which minimizes an algebraic distance:

$$\delta_i = (\mathbf{t}_i - {}^{W}\mathbf{t})^T(\mathbf{t}_i - {}^{W}\mathbf{t}) - r^2$$

Defining $k = {}^{W}\mathbf{t}^T\ {}^{W}\mathbf{t} - r^2$ we solve the following overdetermined equation system:

$$\begin{bmatrix} -2\mathbf{t}_1^T & 1 \\ \vdots & \vdots \\ -2\mathbf{t}_m^T & 1 \end{bmatrix} \begin{bmatrix} {}^{W}\mathbf{t} \\ k \end{bmatrix} = \begin{bmatrix} -\mathbf{t}_1^T\mathbf{t}_1 \\ \vdots \\ -\mathbf{t}_m^T\mathbf{t}_m \end{bmatrix}$$

which is then refined using non-linear minimization, the Levenberg-Marquardt method, of the squared geometric distance:

$$\delta_i^2 = \left(\sqrt{(\mathbf{t}_i - {}^{W}\mathbf{t})^T(\mathbf{t}_i - {}^{W}\mathbf{t})} - r\right)^2$$

Now that we have ${}^{W}\mathbf{t}$ we compute:

$${}^{DRF}\mathbf{t} = \text{mean}(R_i^T[{}^{W}\mathbf{t} - \mathbf{t}_i])$$

2.1.2 Algebraic One Step (AOS)

This formulation is based on the observation that we are pivoting around a fixed point and therefore for all transformations we have:

$$R_i\,{}^{DRF}\mathbf{t} + \mathbf{t}_i = {}^{W}\mathbf{t}$$

We can thus estimate both translations at once by solving the following overdetermined equation system:

$$\begin{bmatrix} R_1 & -I \\ \vdots & \vdots \\ R_m & -I \end{bmatrix} \begin{bmatrix} {}^{DRF}\mathbf{t} \\ {}^{W}\mathbf{t} \end{bmatrix} = \begin{bmatrix} -\mathbf{t}_1 \\ \vdots \\ -\mathbf{t}_m \end{bmatrix}$$

2.1.3 Algebraic Two Step (ATS)

This formulation is again based on the observation that we are pivoting around a fixed point and therefore for any two transformations we have:

$$R_i\,{}^{DRF}\mathbf{t} + \mathbf{t}_i = R_j\,{}^{DRF}\mathbf{t} + \mathbf{t}_j$$

We can thus estimate ${}^{DRF}\mathbf{t}$ by solving the following overdetermined equation system:

$$\begin{bmatrix} R_1 - R_2 \\ \vdots \\ R_{m-1} - R_m \end{bmatrix} \left[{}^{DRF}\mathbf{t}\right] = \begin{bmatrix} \mathbf{t}_2 - \mathbf{t}_1 \\ \vdots \\ \mathbf{t}_m - \mathbf{t}_{m-1} \end{bmatrix}$$

Now that we have ${}^{DRF}\mathbf{t}$ we compute:

$${}^{W}\mathbf{t} = \text{mean}(R_i\,{}^{DRF}\mathbf{t} + \mathbf{t}_i)$$

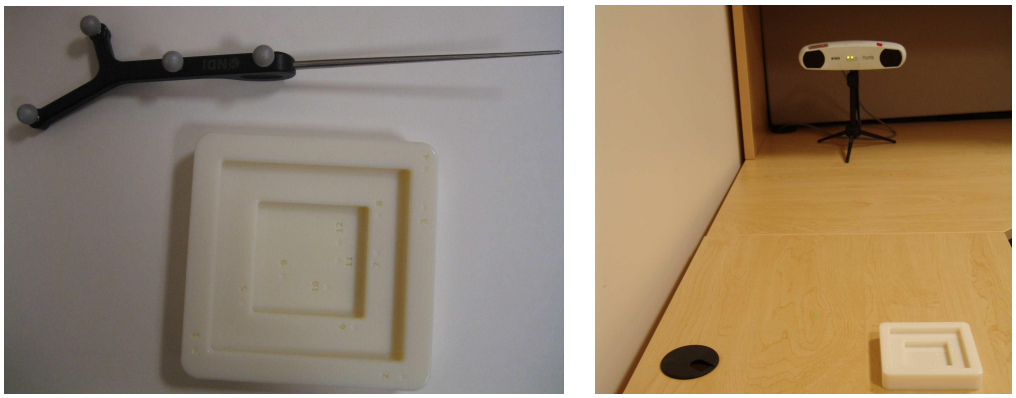

(a) (b)

Figure 2. Experimental setup (a) Optically tracked pointer tool and custom calibration phantom consisting of 12 divot holes at known locations (b) data acquisition in office environment.

2.2 Robust estimation

A characteristic of all the formulations described above is that they have a breakdown point of zero. That is, the result can have an arbitrarily large error even if only a single transformation $[R_i, \mathbf{t}_i]$ is an outlier. This is due to the use of a least-squares approach in all formulations.

One can argue that during calibration the operator ensures that there are no outlying transformations and therefore this scenario is theoretical in nature. In practice, we have experienced instances in which the operator introduces outliers, inadvertently, by moving the pointer tool away from the pivoting point prior to the completion of data acquisition. In this case, if we directly use any of the formulations described above, data acquisition must be repeated. Luckily, robust versions of all three formulations are readily constructed without the need for modifying the original formulations, rather we embed these formulations into a RANSAC framework.[18,19]

To use the RANSAC framework we need three components: a method for parameter estimation using a subset of the data elements, a method for least squares estimation and a function that indicates whether a data element is consistent with a given estimated model.

For the SF formulation we first estimate the sphere center, ${}^{W}\mathbf{t}$, using the RANSAC framework as described in.[17] We then estimate ${}^{DRF}\mathbf{t}$ using transformations whose translational component is part of the consensus set obtained in the previous step. We refer to this estimator as R-SF. For the AOS formulation we use a subset of the transformations to estimate ${}^{W}\mathbf{t}$, and ${}^{DRF}\mathbf{t}$. A transformation, $[R_i, \mathbf{t}_i]$ is consistent with this estimate if $\|R_i {}^{DRF}\mathbf{t} + \mathbf{t}_i - {}^{W}\mathbf{t}\| < \tau, \quad \tau > 0$. Once we obtain the largest consensus set we perform the estimation using the least squares formulation described above. We refer to this estimator as R-AOS. For the ATS formulation we use a similar approach, estimating ${}^{W}\mathbf{t}$, and ${}^{DRF}\mathbf{t}$ using a subset of the transformations, with the final estimate obtained using the least squares formulation applied to the largest consensus set. We refer to this estimator as R-ATS. For all three formulations a data element is considered to be consistent with the estimated model if the relevant distance is less than 1mm (i.e. $\tau = 1.0$).

2.3 Experimental evaluation

To evaluate the accuracy and precision of the different formulations we printed a plastic phantom with 12 divots at known locations. The phantom was printed using the Objet500 Connex 3D printer (Stratasys, MN, USA) which has a manufacturer specified resolution of 0.016mm. We acquire transformations while pivoting a tracked pointer tool at each of the divot locations. In this evaluation we used the Polaris Vicra optical tracking system (Northern Digital Inc., Waterloo, Canada), and the standard pointer tool that is part of the kit that comes with the device. The phantom and pointer tool are shown in Figure 2(a). Data acquisition was carried out in an office environment which allowed us to easily position the tracking system's camera so that there was a direct line of sight to the tracked tool, as shown in Figure 2(b).

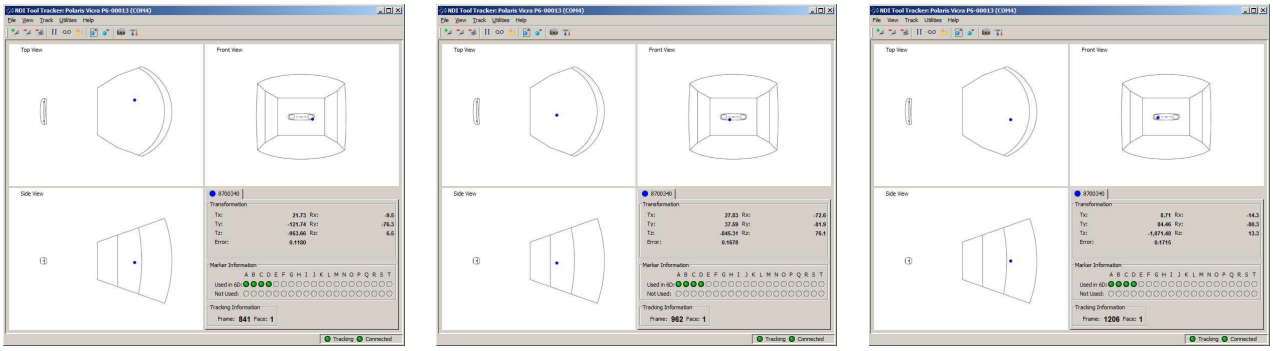

location 1 location 2 location 3

Figure 3. Measurement volume and tool tracking visualization software from NDI showing the position of the DRF in the measurement volume, (blue) sphere, when the pointer was placed in the same divot and directly facing the tracker at the three locations used for data acquisition.

The custom phantom was placed at three locations in the tracker's measurement volume, shown in Figure 3, and the pointer was pivoted in each of the divots for 30sec. Positioning the phantom at several locations in the measurement volume incorporates the spatial variability of tracking accuracy into our evaluation. The process was then repeated, this time deliberately introducing outliers. After 20sec of valid pivot data acquisition the pointer was arbitrarily translated and rotated for the remaining 10sec. In total we acquired 72 datasets, half of which are not contaminated with outliers and half of which have a contamination rate of approximately 30%.

To illustrate that the breakdown point of the least squares based algorithms is indeed zero we arbitrarily selected one of the data sets that has no outliers and added a single outlying transformation to it. We then compared the results of each of the formulations applied to the modified dataset to the result obtained using the AOS formulation applied to the original data.

The location of the pointer tip relative to the DRF, ${}^{DRF}\mathbf{t}$, is not known accurately. This translation is not specified with tight tolerance during manufacturing due to financial costs, and afterwards it may change due to deformation of the tool shaft *. As a consequence, we only evaluated the precision of estimating ${}^{DRF}\mathbf{t}$ based on the distances between the different estimates, $d_{i,j} = \|{}^{DRF}\mathbf{t}_i - {}^{DRF}\mathbf{t}_j\|$.

The locations of the divots are highly accurate from manufacturing. We therefore evaluate the localization accuracy of $\{{}^{DRF}\mathbf{t}_i\}_{i=1..12}$ using rigid registration between the phantom's model and the localized points. In our case we compute the residual distances between the localized points and the transformed model points, $d_i = \|T({}^{P}\mathbf{t}_i) - {}^{W}\mathbf{t}_i\|$.

3. EXPERIMENTAL RESULTS

When we added a single outlier to an outlier free dataset containing 481 transformations, acquired at location 1, it had a significant effect on the least squares estimates, and minor effects on their robust versions. In our case, we established a reference result using the AOS formulation and the outlier free dataset, with the following result, in millimeters, $[{}^{DRF}\mathbf{t}; {}^{W}\mathbf{t}]_{ref} = [-17.78, 1.11, -156.87; 146.90, -62.97, -1042.14]$. The difference between our reference and the estimate obtained with the outlying transformation, $\Delta = \|[{}^{DRF}\mathbf{t}; {}^{W}\mathbf{t}]_{ref} - [{}^{DRF}\mathbf{t}; {}^{W}\mathbf{t}]_i\|$, shows the sensitivity of a method to the presence of a single outlier. The following differences were observed: $\Delta_{SF} = 4068.17$mm, $\Delta_{R-SF} = 0.71$mm, $\Delta_{AOS} = 50.79$mm, $\Delta_{R-AOS} = 0.04$mm, $\Delta_{ATS} = 50.79$mm, $\Delta_{R-ATS} = 0.07$mm. Figure 4 visually illustrates the least squares estimates obtained with a single outlier.

When we combine the results from all three locations, using the outlier free datasets, we see that the algebraic least squares formulations are more precise and accurate than the sphere fitting formulation, and that the two algebraic formulations provide equivalent results. We also observe that the RANSAC framework does not have a detrimental effect when the data is outlier free. That is, embedding the original formulations in the RANSAC

*Private communication with A. D. Wiles, manager advanced research, NDI.

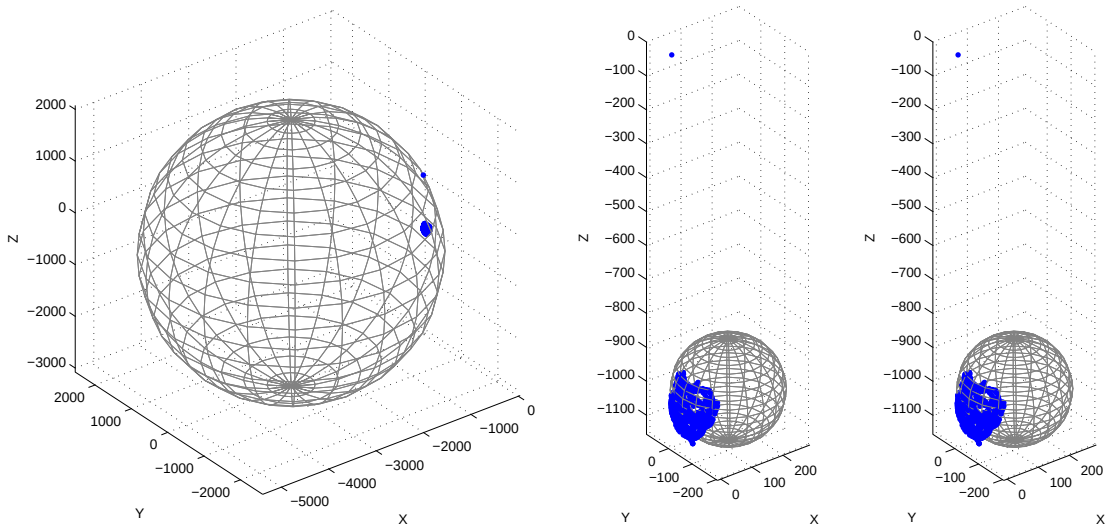

Figure 4. Wireframe sphere constructed using the estimated values for $[{}^{DRF}\mathbf{t}, {}^{W}\mathbf{t}]$, where the sphere center is ${}^{W}\mathbf{t}$, and its radius is $\|{}^{DRF}\mathbf{t}\|$. (Blue) dots are the locations of the DRF used for estimation, the translational component of $[R_i, \mathbf{t}_i]$. In all three cases it is clear that many of the dots are not on the surface of the sphere. In the case of the SF formulation the effect of the outlier is much more pronounced.

framework does not change their performance when the input has no outliers. Not surprisingly, all least-squares formulations break down when evaluated using the datasets containing 30% outliers. On the other hand, their robust versions maintain similar accuracy and precision to those obtained with the outlier free datasets. Table 1 summarizes these results.

We next analyze our results according to the algorithm and the position of the phantom in the tracker's measurement volume. The upper part of Figure 5 summarizes the results for all six algorithms using the outlier free datasets. According to these results it appears that the errors and variability in location 3 are larger than at the two other locations. While the differences between median values are less than 0.2mm, the trend is similar for all formulations. Going back to Figure 3 we see that the difference between the three locations are that location 1 and 2 are closer to the center of the tracker's measurement volume while location 3 is farther away. While the differences are submillimetric it appears that the region within the tracked volume in which calibration is performed has a measurable effect. It should be noted that when we evaluated the formulations using data containing a significant amount of outliers this behavior was no longer consistent.

formulation	clean data		30% outliers	
	${}^{DRF}\mathbf{t}$ variability	${}^{W}\mathbf{t}$ registration error	${}^{DRF}\mathbf{t}$ variability	${}^{W}\mathbf{t}$ registration error
SF	0.35(0.21)	0.25(0.14)	33.21(23.50)	24.89(14.96)
AOS	0.25(0.11)	0.15(0.08)	22.37(11.25)	14.11(7.83)
ATS	0.25(0.11)	0.15(0.08)	22.37(11.25)	14.11(7.83)
R-SF	0.36(0.21)	0.25(0.14)	0.29(0.15)	0.21(0.11)
R-AOS	0.27(0.11)	0.16(0.08)	0.24(0.11)	0.15(0.07)
R-ATS	0.26(0.12)	0.17(0.09)	0.25(0.11)	0.16(0.07)

Table 1. Precision and accuracy, mean(std), of estimating ${}^{DRF}\mathbf{t}$ and ${}^{W}\mathbf{t}$. All results are in millimeters. The robust versions of the least squares formulations provide similar results to the standard least squares formulations on data that has no outliers and are not affected by the significant number of outliers in the contaminated datasets.

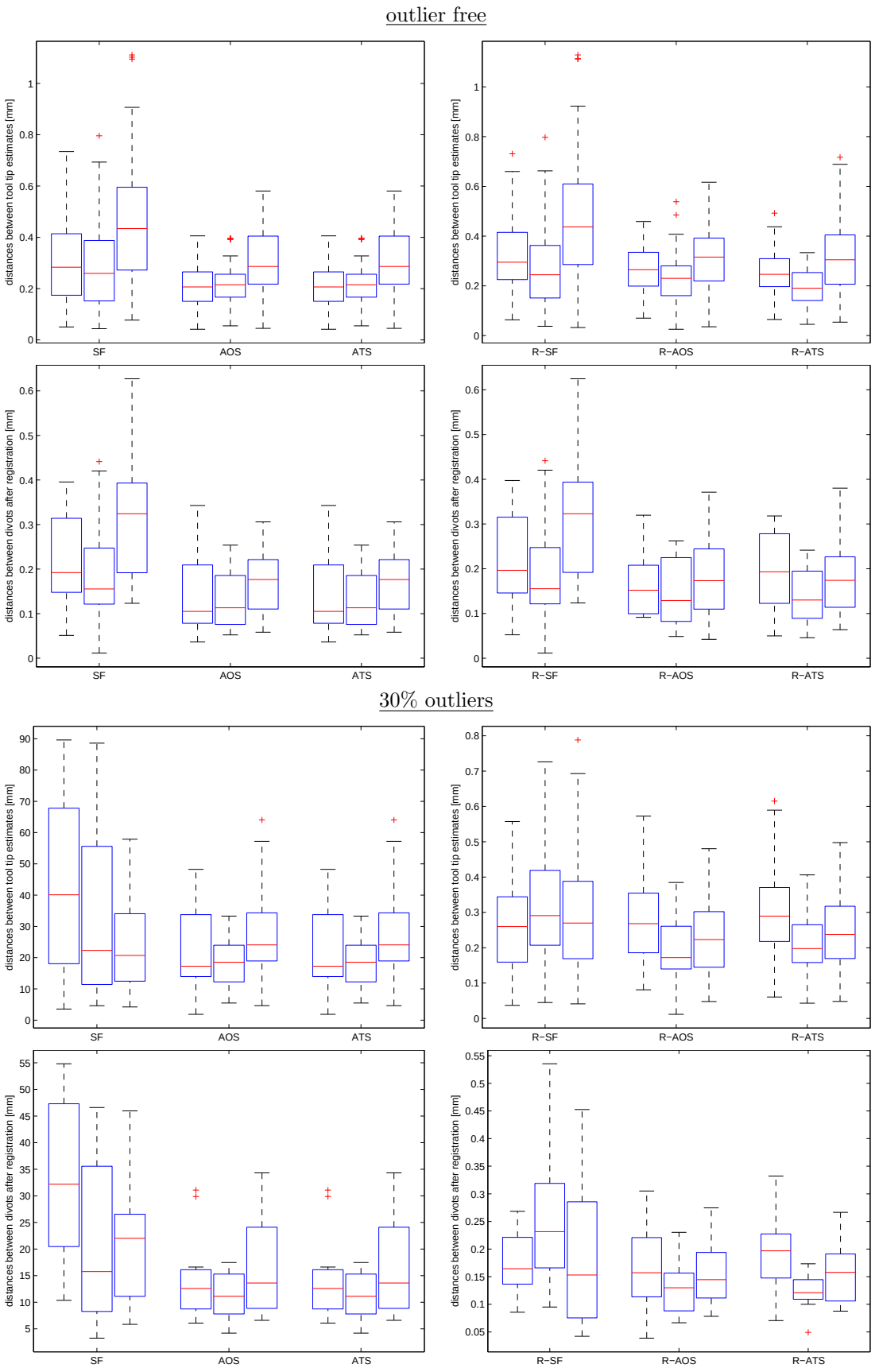

Figure 5. Experimental results divided according to the three data acquisition locations and algorithms. (first and third row from the bottom) accuracy of registration based on the accuracy of localizing ${}^{W}\mathbf{t}$; (second and forth row from the bottom) variability in estimating ${}^{DRF}\mathbf{t}$.

The lower part of Figure 5 summarizes the results for all six algorithms using the datasets containing 30% outliers. Note that in this case the results obtained by the standard least squares formulations are irrelevant, and that their robust versions readily dealt with the high number of outliers.

4. DISCUSSION AND CONCLUSIONS

The use of a pivoting motion to localize points with respect to a DRF and with respect to a world coordinate system is a widely used approach. Among others, it has been utilized for localization of the tip of pointer tools, robotic end effectors, haptic styluses, and for localizing the center of anatomical spherical joints. These applications of pivot calibration have been previously described in a large number of publications, a sampling of which were presented in the introduction. While the task of pivot calibration is well defined, the resulting numerical estimates are potentially dependent on the mathematical formulation used to obtain the solution. In this work we empirically evaluated the performance of three formulations using an optically tracked pointer tool.

As all evaluated formulations use a least squares approach, they are not robust to outliers. We have shown that for all of the formulations a single outlier can render the results useless. We have also shown that embedding each of the formulations into the RANSAC framework makes them robust to outliers, with stable and accurate results obtained even when the data contained a large amount of outliers (30% contamination rate).

When evaluating the performance of the three formulations we observed that the algebraic formulations, AOS and ATS, have equivalent performance and that it is superior to the performance of the geometric, SF, formulation. We have shown that the SF approach yields tool calibration estimates, ${}^{DRF}\mathbf{t}$, that are less precise than the algebraic formulations, and that it also yields divot localizations, ${}^{W}\mathbf{t}_i$, that are less accurate. In addition, we observed that the location inside the tracker's measurement volume has a measurable effect on the precision and accuracy of the results. For optimal results calibration should be performed close to the center of the measurement volume. While this conclusion is valid for outlier free data, the effect of the location was not measurable when the data contained a significant amount of outliers.

Based on our results we conclude that the three commonly used mathematical formulations for obtaining estimates using pivot calibration are not equivalent. We therefor recommend the use of the algebraic formulations over the SF formulation.

ACKNOWLEDGMENTS

We thank Emmanuel Wilson for his help with the design and printing of the calibration phantom.

REFERENCES

[1] Jaramaz, B., Nikou, C., Simon, D. A., and DiGioia III, A. M., "Range of motion after total hip arthroplasty: Experimental verification of the analytical simulator," in [*CVRMed-MRCAS'97*], 573–582 (1997).

[2] Birkfellner, W., Watzinger, F., Wanschitz, F., Ewers, R., and Bergmann, H., "Calibration of tracking systems in a surgical environment," *IEEE Trans. Med. Imag.* **17**(5), 737–742 (1998).

[3] Khamene, A. and Sauer, F., "A novel phantom-less spatial and temporal ultrasound calibration method," in [*Medical Image Computing and Computer-Assisted Intervention*], 65–72 (2005).

[4] Boctor, E. M., Fichtinger, G., Taylor, R. H., and Choti, M. A., "Tracked 3D ultrasound in radio-frequency liver ablation," in [*SPIE Medical Imaging: Ultrasonic Imaging and Signal Processing*], (2003).

[5] Magee, D., Zhu, Y., Ratnalingam, R., Gardner, P., and Kessel, D., "An augmented reality simulator for ultrasound guided needle placement training," *Med Biol Eng Comput.* **45**(10), 957–967 (2007).

[6] Yaniv, Z., Cheng, P., Wilson, E., Popa, T., Lindisch, D., Campos-Nanez, E., Abeledo, H., Watson, V., Cleary, K., and Banovac, F., "Needle-based interventions with the image-guided surgery toolkit (IGSTK): From phantoms to clinical trials," *IEEE Trans. Biomed. Eng.* **57**(4), 922–933 (2010).

[7] Harders, M., Bianchi, G., Knoerlein, B., and Székely, G., "Calibration, registration, and synchronization for high precision augmented reality haptics.," *IEEE Trans. Vis. Comput. Graph.* **15**(1), 138–149 (2009).

[8] Kienzle Ill, T. C., Stulberg, D., Peshkin, M., Quaid, A., Lea, J., Goswami, A., and Wu, C.-H., "Total knee replacement," *IEEE Eng. Med. Biol. Mag.* **14**(3), 301–306 (1995).

[9] Lea, J. T., Watkins, D., Mills, A., Peshkin, M. A., Kienzle III, T. C., and Stulberg, S. D., "Registration and immobilization in robot-assisted surgery," *Image Guided Surgery* **2**(1), 80–87 (1995).

[10] Leitner, F., Picard, F., Minfelde, R., Schulz, H.-J., Cinquin, P., and Saragaglia, D., "Computer-assisted knee surgical total replacement," in [*Computer Vision, Virtual Reality and Robotics in Medicine and Medical Robotics and Computer-Assisted Surgery (CVRMed-MRCAS)*], 19–22 (1997).

[11] Delp, S. L., Stulberg, S. D., Davies, B., Picard, F., and Leitner, F., "Computer assisted knee replacement," *Clin Orthop Relat Res.* **354**, 49–56 (1998).

[12] Mizuno, T., Ryuichi, H., and Nishi, H., "Method for automatically setting a tool tip point." US Patent 4,979,127 (1990).

[13] Baron, S., Eilers, H., Munske, B., Toennies, J. L., Balachandran, R., Labadie, R. F., Ortmaier, T., and Webster III, R. J., "Percutaneous inner-ear access via an image-guided industrial robot system," *Proc Inst Mech Eng H.* **224**(5), 633–649 (2010).

[14] Tovar-Arriaga, S., Vargas, J. E., Ramos, J. M., Aceves, M. A., Gorrostieta, E., and Kalender, W. A., "A fully sensorized cooperative robotic system for surgical interventions," *Sensors* **12**(7) (2012).

[15] Detmer, P. R., Bashein, G., Hodges, T., Beach, K. W., Filer, E. P., Burns, D. H., and Strandness Jr., D. E., "3D ultrasonic image feature localization based on magnetic scanhead tracking: in vitro calibration and validation," *Ultrasound Med Biol. 1994;20(9):923-36.* **20**(9), 923–936 (1994).

[16] Schreiner, S., Galloway Jr., R. L., Lewis, J. T., Bass, W. A., and Muratore, D. M., "An ultrasonic approach to localization of fiducial markers for interactive, image-guided neurosurgery-part II: Implementation and automation," *IEEE Trans. Biomed. Eng.* **45**(5) (1998).

[17] Yaniv, Z., "Localizing spherical fiducials in C-arm based cone-beam CT," *Med. Phys.* **36**(11), 4957–4966 (2009).

[18] Fischler, M. A. and Bolles, R. C., "Random sample consensus: a paradigm for model fitting with applications to image analysis and automated cartography," *Commun. ACM* **24**(6), 381–395 (1981).

[19] Yaniv, Z., "Random sample consensus (RANSAC) algorithm, a generic implementation," *Insight Journal* **July-December** (2010).